Retrieval of chlorophyll fluorescence from reflectance spectra through polarization discrimination: modeling and experiments

Alexander Gilerson, Jing Zhou, Min Oo, Jacek Chowdhary, Barry M. Gross, Fred Moshary, and Samir Ahmed

The polarization discrimination technique we recently developed, shows that it is possible to separate the elastic scattering and the chlorophyll fluorescence signal from the water-leaving radiance by making use of the fact that the elastically scattered components are partially polarized, while the fluorescence signal is unpolarized. The technique has been shown to be applicable to a wide range of water conditions. We present an extension of experimental and analytical results, which serve to define the scope of this technique and its range of applicability. A new analysis, based on vector radiative transfer computations, and on laboratory and field measurements on eastern Long Island and in the Chesapeake Bay, shows that the technique is generally effective for both open ocean and coastal waters, but that it is limited if the ocean bottom albedo and/or multiple scattering due to very high mineral particle concentrations result in depolarizing the water-leaving radiance. In addition, we show that in contrast with the polarization-based retrieval, the traditional method of extracting fluorescence height using the baseline method can give significant errors, particularly for coastal waters where it strongly overestimates the fluorescence values.

OCIS codes: 280.0280, 290.0290, 300.0300.

1. Introduction

The development of algorithms for the retrieval of chlorophyll *a* concentrations [Chl] in the coastal zone from remote sensing spectra is frequently based on the analysis of spectral features in the near infrared[1–5] (NIR) since the simple blue-green ratio approach, which is valid in open oceans, fails when strongly scattering mineral particles and color dissolved organic matter (CDOM) are present. However, the reflectance peak in the NIR can be significantly affected by chlorophyll fluorescence depending on the water composition.[6] The accuracy of [Chl] retrieval depends, therefore, on the ability to separate contributions of elastic scattering from fluorescence spectra in the NIR reflectance. Both contributions can vary significantly in case 1 (open) waters, where the underwater light properties are predominantly determined by phytoplankton and their by-products,[1] and in case 2 (coastal) waters, where mineral particles and CDOM can substantially affect scattering and absorption.[7–10]

Independent measurements of chlorophyll fluorescence and [Chl] can provide additional insight into photosynthetic activity and variability of fluorescence quantum yield, which can be linked to the differences in species, nutrient supply, and ambient light levels.[11] Fluorescence as a first approximation can be considered as a measure of [Chl] if reasonable assumptions can be made about fluorescence quantum yield values.[1] Fluorescence measurements can also help in the detection of harmful algae blooms.[12] Therefore improvements in the detection of fluorescence, especially by means of remote sensing, provide additional possibilities in several fields of study.

Solar stimulated chlorophyll fluorescence has been accurately measured using Fraunhofer line discrimination[13] with high resolution monochromators. Other approaches include, for instance, a series of bandpass filters to separate elastic and inelastic components,[14] and dual monochromators with sources and detectors

A. Gilerson, J. Zhou, M. Oo, B. M. Gross, F. Moshary, and S. Ahmed (ahmed@ccny.cuny.edu) are with the Optical Remote Sensing Laboratory, Department of Electrical Engineering, The City College of the City University of New York, New York, New York 10031. J. Chowdhary is with the Department of Applied Physics and Applied Mathematics, Columbia University, New York, New York 10025.

Received 4 November 2005; revised 12 March 2006; accepted 14 March 2006; posted 20 March 2006 (Doc. ID 65755).
0003-6935/06/225568-14$15.00/0

selectively tuned over appropriate spectral ranges to measure true elastic reflectance.[15] However, none of these methods is well suited to remote sensing. Approximate fluorescence retrievals were obtained through the inversion of reflectance spectra[16] but different models have been used to assess the impact of fluorescence on total reflectance,[11,17,18] showing that theoretical prediction of the fluorescence magnitude is difficult due to the large variability of the water compositions.

In recent papers describing the polarization discrimination technique,[19–21] it was shown that it is possible to separate the elastic scattering and the chlorophyll fluorescence signal from the water-leaving radiance by making use of the fact that the elastically scattered component is partially polarized, while the fluorescence signal is unpolarized. The technique's validity was initially confirmed through excellent agreement between the spectral shape of fluorescence extracted in this manner and the laser-induced fluorescence of the same species.

The approach presented here shows the efficacy of the technique for a variety of water conditions, including the addition of high concentrations of clay in test samples, and for rough water conditions as long as sufficient temporal (or spatial) averaging is performed. The technique has also been successfully tested during *in situ* field measurements on eastern Long Island and in the Chesapeake Bay. It was found that the efficacy of the fluorescence retrieval depends on the degree of polarization of the water-leaving radiance and the near linearity of the relationship between the two orthogonal polarization components of the elastically scattered light over the limited spectral range in the vicinity of the fluorescence spectral band. We present a set of experimental and numerical results that updates previous work and serves to define the scope of this technique and its range of applicability to open and coastal waters. The numerical results are based on radiative transfer (RT) computations of polarized light in atmosphere–ocean systems,[22] while new experimental results are presented for laboratory and field measurements.

The laboratory results presented demonstrate the robustness of the polarization discrimination technique and its applicability to different types of algae, for a wide variety of illumination and water conditions, including high mineral particle concentrations (TSS), rough surface water conditions, and natural sunlight. Furthermore, the laboratory methodology has also been applied to field measurements and a RT-based analysis is carried out to examine if these results can be replicated by simulations, and to theoretically evaluate the scope and limitations of the technique. In particular, we explore how the degree of linear polarization contributes to the quality of the fluorescence retrieval. This is achieved by superimposing a reasonable level of unpolarized fluorescence onto the RT calculated elastic reflectance spectrum and applying the polarization discrimination procedure to retrieve the fluorescence component. The simulations show that the polarization-based fluorescence retrieval works generally well for both open and coastal waters, but that it may be limited if the ocean bottom albedo and/or particularly high TSS multiple scattering depolarizes the water-leaving radiance. In addition, the retrievals obtained by polarization discrimination are more accurate than traditional baseline methods, which make use of the unpolarized reflectance spectrum. This is because the latter cannot properly decouple the effects of chlorophyll fluorescence and absorption (as is done by the polarization discrimination technique). In particular, we show that the baseline fluorescence extraction method strongly overestimates fluorescence value for coastal waters. Finally, it should be noted that the polarization properties of the reflectance spectra obtained here are also of intrinsic interest because of their potential for constraining the remote sensing retrievals of both aerosols and ocean particulates.[23,24]

2. Main Features of the Polarization Discrimination Technique

A. Basic Quantities

The premise of the technique is based on the fact that light elastically scattered by algae will show various degrees of linear polarization depending on the polarization of the incident light and on the scattering angle,[25] whereas fluorescence excited and emitted by these same algae is always unpolarized.[26] Thus if a polarizer is placed in front of a probe that is used to measure the reflectance of scattered light, then rotating the polarizer will cause the reflectance of measured intensity to vary from a minimum $R_{\min}$ to a maximum $R_{\max}$. These reflectances can be decomposed into signal components $R_{\|}$ and $R_{\perp}$ that are polarized parallel and perpendicular to the scattering plane, respectively, plus half of the reflectance fluorescence (Fl) caused by a chlorophyll fluorescence band at 685 nm with a FWHM of 25 nm. That is,

$$R_{\max}(\lambda) = R_{\perp}(\lambda) + 0.5\mathrm{Fl}(\lambda), \tag{1}$$

$$R_{\min}(\lambda) = R_{\|}(\lambda) + 0.5\mathrm{Fl}(\lambda), \tag{2}$$

where λ is the wavelength of scattered light. The total signal $R(\lambda)$ is given by

$$R(\lambda) = R_{\max}(\lambda) + R_{\min}(\lambda) = R_{\perp}(\lambda) + R_{\|}(\lambda) + \mathrm{Fl}(\lambda), \tag{3}$$

and the sum of the elastically scattered polarized components by

$$R_s(\lambda) = R_{\perp}(\lambda) + R_{\|}(\lambda). \tag{4}$$

B. Polarized Illumination

We first examine the special case shown in the experimental arrangement of Fig. 1(a), where the illumination is polarized perpendicular to the scattering plane (i.e., the plane spanned by the directions of

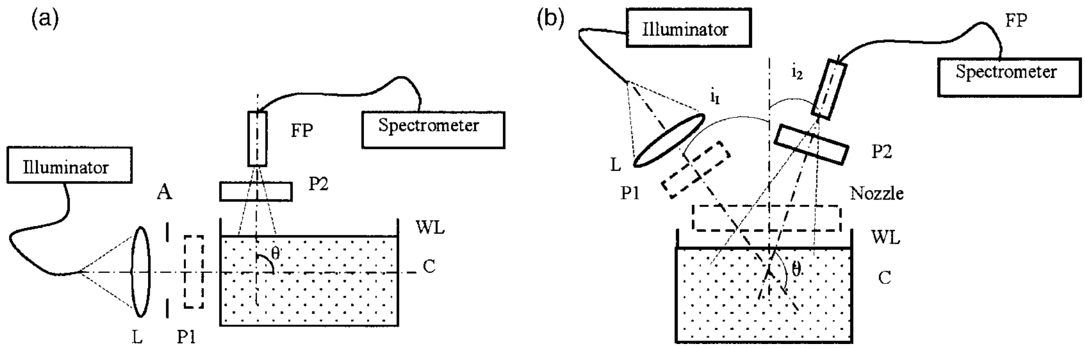

Fig. 1. Experimental setup. (a) Detector perpendicular to the axis of illumination, (b) general case of illumination and detection. L, lens; FP, fiber probe; A, aperture; P1, P2, polarizer and analyzer; C, cuvette with algae; WL, water level.

illumination and detection). If we consider single scattering only and neglect any depolarization caused by the finite numerical aperture, then the elastically scattered light will be polarized in the same direction and $R_{\|}(\lambda)$ will be zero.[25] Under these conditions, Eq. (2) reduces to

$$\mathrm{Fl}(\lambda) \approx 2R_{\min}(\lambda). \quad (5)$$

The total elastic component $R_s(\lambda)$ is then obtained by subtracting the fluorescence $\mathrm{Fl}(\lambda)$ from the total reflectance Eqs. (3) and (4).

C. Unpolarized Illumination

Next we consider the more general case of unpolarized illumination. If the incident beam of light is unpolarized, then Eq. (3) would, along with component $R_{\perp}(\lambda)$, also have a significant nonzero component $R_{\|}(\lambda)$. In our previous work,[19] we showed that there exists a strong linear correlation between $R_s(\lambda)$ and the difference signal $R_d(\lambda)$ given by

$$R_d(\lambda) = R_{\max}(\lambda) - R_{\min}(\lambda) = R_{\perp}(\lambda) - R_{\|}(\lambda). \quad (6)$$

Note that the fluorescence components are eliminated in Eq. (6) as a result of subtracting $R_{\min}(\lambda)$ from $R_{\max}(\lambda)$. If the correlation between $R_d(\lambda)$ and $R_s(\lambda)$ extends into the fluorescence zone, then one can easily extract the fluorescence using Eqs. (3) and (4),

$$\mathrm{Fl}(\lambda) = R(\lambda) - R_s(\lambda). \quad (7)$$

More precisely, assuming that $R_d(\lambda)$ and $R_s(\lambda)$ are linearly correlated for elastic scattering, we fit $R_d(\lambda)$ onto $R(\lambda)$ in the 450−670 nm range (i.e., outside the fluorescence spectral region) using linear regression. The regression parameters are then used to extract $R_s(\lambda)$ from $R_d(\lambda)$ for the wavelength range of 670−750 nm, after which Eq. (7) is applied to obtain $\mathrm{Fl}(\lambda)$. It should be noted that the linearity of $R_s(\lambda)$ and $R_d(\lambda)$, over a limited spectral domain surrounding the fluorescence band where the linear regression is performed, has been validated both experimentally and theoretically.[19,27] This linearity also leads to the relationship

$$R_{\max}(\lambda) - 0.5\mathrm{Fl}(\lambda) = [R_{\min}(\lambda) - 0.5\mathrm{Fl}(\lambda)]A + B, \quad (8)$$

where A and B are the regression parameters for the fit of $R_{\|}(\lambda)$ into $R_{\perp}(\lambda)$ in the spectral zones outside the fluorescence region. Equation (8) provides yet another expression for $\mathrm{Fl}(\lambda)$ in terms of $R_{\min}(\lambda)$ and $R_{\max}(\lambda)$, i.e.,

$$\mathrm{Fl}(\lambda) = 2[AR_{\min}(\lambda) + B - R_{\max}(\lambda)]/(A - 1). \quad (9)$$

Equations (8) and (9) were used for the retrieval of fluorescence in cases where $R_{\max}(\lambda)$ and $R_{\min}(\lambda)$ were so close to one another that $R_d(\lambda)$ is only slightly above the noise level.

3. Experimental Results

A. Experimental Setup

Experiments were carried out with both polarized and unpolarized sources, including sunlight, both in the laboratory and in the field. The basic laboratory experimental setup is shown in Fig. 1. White light from a 150 W lamp (PL-900 Dolan Jenner) illuminator or from a 150 W quartz halogen lamp (Cuda Corporation) illuminator is used to illuminate seawater containing algae through a fiber-optic light guide, lens, and an optional polarizer, P1 (used in some of the experiments). The seawater containing the algae is placed in the cuvette C. The test sample is illuminated at different angles i_1 directly [Fig. 1(b)] or through clear glass on the side of the cuvette when $i_1 = 90°$ [Fig. 1(a)]. All other cuvette surfaces are covered with black tape to minimize spurious reflections. The collection optics, consisting of a fiber-optic probe (multimode fiber with 200 μm core diameter) coupled to an SQ-2000 fiber optic (Ocean Optics) spectrometer, collects the elastically scattered or reflected and fluorescence light from the illuminated site with geometries such that the light is captured over a 24° angle in the air (the fiber numerical aperture is 0.22). The fiber probe is installed vertically above the surface of the water or at the angle i_2 to the vertical direction. A rotating polarizer P2 is placed in front of the probe. All the measured spectra were referenced to a Spectralon reflector from Labsphere. To create a rough water surface for the laboratory measurements, air from a fan at different speeds was directed along the surface of the water through a

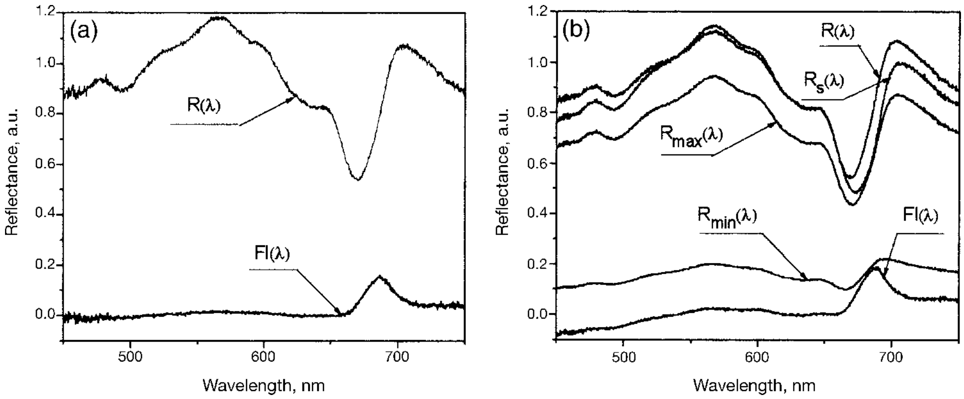

Fig. 2. Detected and processed spectra for the experiments with the algae *Thalassiosira weissflogii.* (a) Polarized light source and (b) unpolarized light source.

rectangular nozzle positioned ~200 mm from the cuvette. The value of the wind speed near the water surface was estimated using a Pitot tube and water piezometer. Experiments were also carried out with sunlight illumination on the roof of the City College of New York building with cultured algae. Field experiments were carried out in the bays of eastern Long Island and in Chesapeake Bay.

B. Algae with Different Shape and Size of the Particles

We previously[19] reported results for two types of near spherical algae: *Isochrysis sp*., which are largely spherical approximately 5 μm diameter, and algae *Tetraselmis striata*, which are slightly elliptical approximately 12 μm diameter; both algae were tested at concentrations $\sim 10^6$ cells/ml. Here we report on additional algae. *Thalassiosira weissflogii* have the shape of rectangular plates with sizes of 8–10 × 14–18 μm, and "*Pavlova*," which are close to spherical with sizes around 10 μm. The concentrations were $2-4 \times 10^6$ for both types of algae.

The results for the algae *Thalassiosira weissflogii* are shown in Fig. 2. Although the shape of the algae particles is far from spherical, fluorescence was successfully extracted using the experimental arrangements of Fig. 1 with both polarized and unpolarized sources and the linear regression procedures discussed in Section 2 above. It can be seen that the ratio of the fluorescence maximum and the maximum of the total reflectance curve (near 570 nm) can vary for polarized and unpolarized illumination since fluorescence is proportional to the intensity of the incident light but reflectance also depends on the phase functions for perpendicular and parallel polarized light, which are generally different. Similar results to those shown in Fig. 2 were also obtained for the algae *Pavlova.* Comparisons of the extracted fluorescence shape with the shape of laser-induced fluorescence with a peak at 685 nm and width at half-maximum approximately 25 nm has been discussed previously (for the algae *Isochrysis sp.*)[19] and showed an excellent match. The shapes of fluorescence extracted are similar to those obtained by other researchers.[11] Asymmetric deviations from a simple Gaussian, particularly at the long end of the spectrum may be due to a combination of effects: increasing algal self-absorption and elastic reflectance, rapidly increasing water absorption, and inaccuracies in the fluorescence signal retrieval process in a spectral region of decreasing signal-to-noise ratio.

C. Experiments With Dilution of Algae and With Different Angles of Illumination

Figure 3 shows the fluorescence curves extracted for various algae concentrations using unpolarized illumination. The fluorescences obtained were successfully extracted as the test samples were diluted down to concentrations as low as 1/250 of the original concentration corresponding to about 1 mg/m^3 (not shown on the graph because of the small value).

Results for extracted fluorescence in the dilution experiments for both unpolarized and polarized illumination are presented in Fig. 4. They show similar results for both types of illumination and confirm the validity of the polarization discrimination technique. Concentrations and fluorescence magnitudes are normalized, respectively, to the original concentration of algae and fluorescence magnitude, and the initial maximum [Chl] concentration was approximately 300 mg/m^3. The resultant dilution curves show that

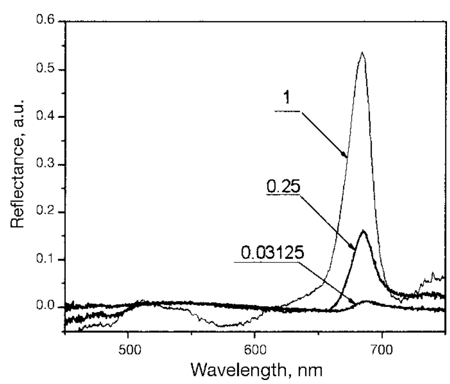

Fig. 3. Fluorescence extracted in the unpolarized illumination setup for different concentrations of algae *Pavlova*. Numbers on the graph are relative concentrations.

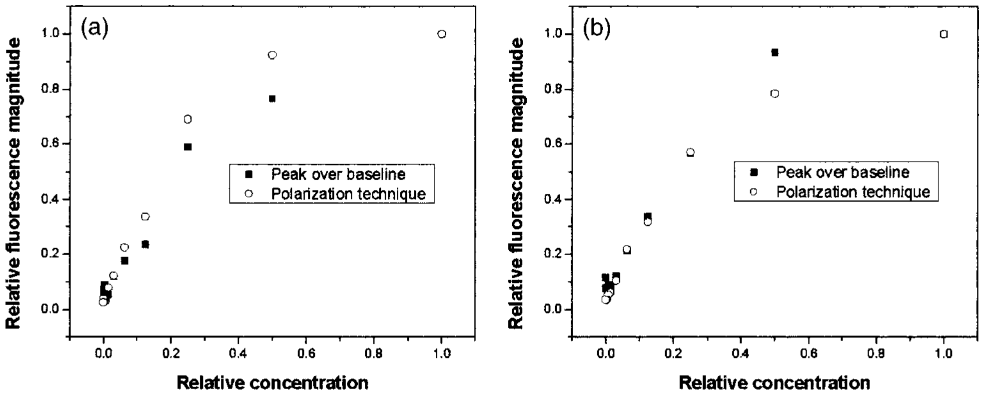

Fig. 4. Comparison of different methods of Chl fluorescence extraction from reflectance spectra for various [Chl]: algae *Tetraselmis striata*: (a) unpolarized light and (b) polarized light.

some saturation exists at the higher concentrations of about 75 mg/m^3 for both polarized and unpolarized sources with similar qualitative results for other types of algae. In comparison, Babin *et al.*[11] observed saturation at considerably lower [Chl] values. Differences in the experimental saturation level may be understood by noting that the probable saturation mechanisms are self-absorption effects that are influenced by the specific field conditions,[11] including possible mineral scattering and other absorption processes, as well as different types of algae, in contrast with the conditions of our laboratory measurements and the cultured algae used in them.

The potential for fluorescence extraction was also tested under laboratory conditions for different angles of illumination i_1 [see Fig. 1(b)] with the detection probe in the vertical position, for both polarized and unpolarized light sources. For polarized illumination, it was found that determination of the fluorescence was reliable for the range of incident angles from 30° to 70°. While the amplitudes of the reflectance curves and the magnitudes of the fluorescence peaks were different due to the differences in the sensor field of view, the shape of the extracted fluorescence was the same with a peak at 685 nm and was negligible outside the fluorescence zone.

Extraction of fluorescence for unpolarized light was less accurate but still reasonable for angles of illumination $i_1 = 30°-50°$. Similar results were obtained with the same algae and sunlight illumination.

D. Comparison of the Fluorescence Retrieval with Polarization Discrimination Technique with Other Methods as a Function of [Chl] Concentration

Since the polarization discrimination technique provides a method for the determination of the magnitude of [Chl] fluorescence, it is interesting to compare these results with the other fluorescence estimation methods. This comparison was done for three types of algae: *Isochrysis, Tetraselmis striata*, and *Pavlova* with illumination at $i_1 = 90°$. The magnitude of fluorescence extracted with both polarized and unpolarized light sources was compared with the magnitude of the fluorescence obtained through the baseline method.[28] In this method, a baseline was created by drawing a line between points on reflectance curves at 665 and 746 nm, and fluorescence height was determined to be the difference between the reflectance and the baseline value at 677 nm. For one type of algae, *Isochrysis*, we also measured peaks over baseline for the reflectance curves acquired by the direct immersion into the algal waters of a fiber-optic probe that had six circumferential fibers for illumination around one fiber in the center for detection. For these experiments, algal waters with original concentrations higher than 10^6 cells/ml ([Chl] $\sim$ 300 mg/m^3) were diluted up to 1000 times, and all concentrations and magnitudes were normalized to their respective values at the original concentration. Results for different types of algae are shown in Figs. 4 and 5.

It is seen in these results that the normalized magnitudes of fluorescence extracted by polarization discrimination match very well those obtained by the baseline method, including the independent experiments using the probe submerged into the water for the algae *Isochrysis* in Fig. 4. It should be noted that these results apply to measurements in the absence of scattering contributions from mineral particles. When these effects are taken into account, as discussed in Section 4, the baseline method is unable to isolate the fluorescence.

E. Surface Roughness Effects

Laboratory experiments were also conducted to examine in a simple fashion the influence of the wind and resulting surface roughness on the polarization retrieval technique. The air from a fan through a rectangular nozzle was directed to the surface of the seawater containing the algae. The water level for these experiments was kept close to the edges of the cuvette. Experiments were carried out with the detector in the vertical position at different heights above the surface of the water. The speed W of the wind above the water surface was varied between 0 and 9.5 m/s.

The angle i_1 of incident light [Fig. 1(b)] was fixed at 45°. For the windy conditions, we increased time of signal averaging from the typically 10 ms to 100 ms.

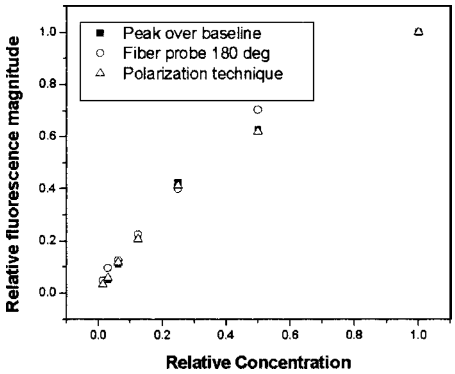

Fig. 5. Comparison of different methods of Chl fluorescence extraction from reflectance spectra for various [Chl]: algae *Isochrysis sp.*; unpolarized light.

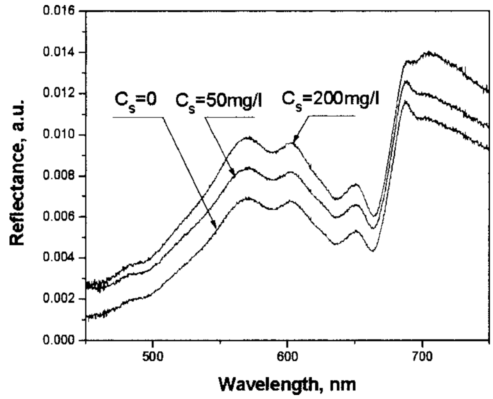

Fig. 7. Reflectance curves for algae with clay, $C_s = 0$ to 200 mg/l .

The resulting change in acquisition time of one complete spectrum increased from 1 to 2 s to 10 s, which appeared to be sufficient for the proper averaging of surface fluctuations due to wind.

Both polarized and unpolarized sources of illumination were used for the experiments; the results for the polarized source are shown in Fig. 6. It is observed that the polarization-based extraction of fluorescence remains accurate with surface wind despite the divergence effects of surface waves.[29] The results with an unpolarized source of illumination were similar. The potential to retrieve fluorescence signals from measurements above the water surface even if the surface wind is large is consistent with recent findings that the surface roughness has little effect on the reflectance of water-leaving radiances.[30] It should further be noted that observations made at higher altitudes (e.g., from an aircraft) would be spatially averaged and therefore lead to similar results as those obtained by time averaging.

F. Algae With Clay

Mineral particles are inherent in all water compositions, can exist in high concentrations in coastal waters, and are a main source for backscatter and reflectance because of their relatively higher refractive index. They also can increase the effects of multiple scattering and substantially affect the degree of polarization. The following experiments were carried out to estimate the influence of mineral particles on the extraction of fluorescence.

In these experiments, cultured algae *Isochrysis sp.* with chlorophyll a concentration [Chl] = 400 mg/m^3 were used. The high algae concentration minimized the effects of the cuvette's bottom. Different concentrations of clay Na–montmorillonite from 10 to 100 mg/l were added to the algae, and fluorescence was extracted using the polarization technique with both polarized and unpolarized illumination. Representative total reflectance spectra for different clay concentrations with unpolarized illumination are shown in Fig. 7. In Fig. 8, one can follow the fluorescence extraction process with polarization components for clay concentration $C_s = 100$ mg/l. It is seen that there is a significant nonzero component in the fluorescence spectrum in the blue–green, which is due to a slight nonlinearity between polarization components amplified by the retrieval process. However, both experiments and calculations show that this nonlinearity does not materially affect [Chl] fluorescence extraction in the 685 nm zone. In particular, the extracted [Chl] fluorescence is very clearly identified, and fluorescence

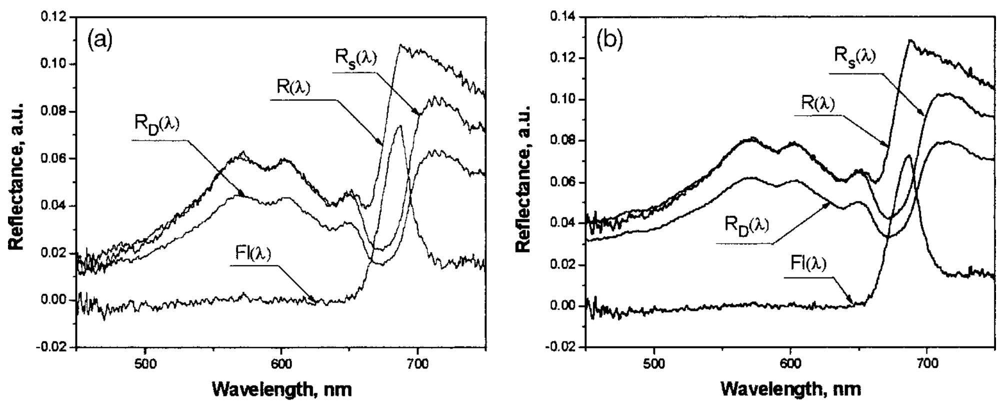

Fig. 6. Influence of the wind on the extraction of fluorescence with polarized light source (probe vertical, 50 mm above water surface): (a) no wind and (b) wind speed near water surface ~9.5 m/s.

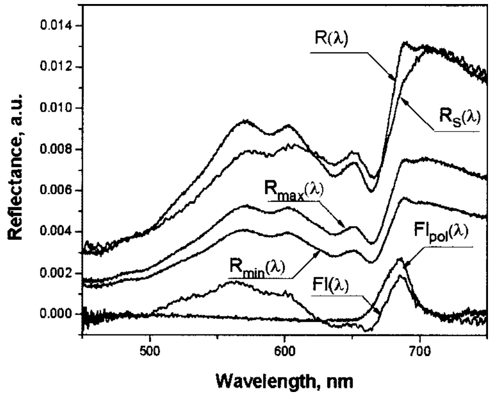

Fig. 8. Fluorescence retrieval from algae with clay, C_s = 100 mg/l.

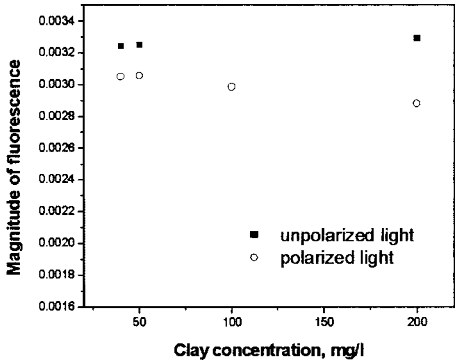

Fig. 9. Fluorescence magnitude retrieved from algae with different concentrations of clay.

retrieved from both polarized and unpolarized illumination shows a reasonably good match.

The results of fluorescence retrieval for different clay concentrations with polarized and unpolarized light are shown in Fig. 9. For clay concentrations up to 200 mg/l, the fluorescence is constant to within ±10%. Above this region, depolarization through extreme multiple scattering inhibits useful retrieval.

G. Field Measurements

Field measurements were conducted in coastal areas of the Shinnecock and Peconic Bays, Long Island, New York, in June 2004, and in the Chesapeake Bay in July 2005. Chlorophyll concentrations [Chl] were measured by a SeaTech fluorometer on Long Island, and by a chlorophyll fluorescence channel on a WETLABS bb9 instrument in the Chesapeake Bay. Reflectance was measured with a GER 1500 spectroradiometer with different Sun angles with a fiber-optic probe in the vertical position as well as at different viewing angles. Figure 10(a) shows an example of spectra obtained from measurements on Long Island with the probe in the vertical position above the water, a solar zenith angle of 61° and [Chl] concentrations estimated at 8 mg/m^3 from fluorometer measurements. Spectra in Fig. 10(b) were obtained in the Chesapeake Bay with the probe just below the water and [Chl] = 41 mg/m^3 (as estimated from fluorometer measurements). Similar spectra were obtained for above-water measurements at the same point (and showed, as expected, similar ratios of fluorescence to reflected amplitudes).

In considering above-water and in-water measurements, it should be noted that skylight reflectance, i.e., sky glint, and sunglint will contribute to polarization in the reflectance signal for measurements made above the water. Direct sunglint can be largely avoided by the appropriate choice of viewing angle and direction with respect to the solar illumination. Some polarized signals will remain due to sky glint and a smaller residual component of sunglint due to surface roughness. However, since the skylight spectral dependence is well characterized through independent measurements made at each site, we correct for it by fitting the measured spectra to the skylight spectra in the deep blue spectral windows where it is dominant. At this point, the sky glint contribution is subtracted from the signals at each polarization before using them for fluorescence extraction (depending on the viewing angle, even vertical orientation of the polarizer does not completely eliminate possible effects of sky glint, and the fitting subtraction procedure remains necessary). The small residual sunglint due to Fresnel reflections resulting from surface waves is close to wavelength independent,[31] and since the measurement procedure followed here normalizes the reflectance at both polarizations with respect to incident sunlight, the residual sunglint contribution will result in a constant wavelength-independent shift in each of the measured spectra, with neutral impact on the linear fitting procedure and the subsequent extraction of fluorescence. The impact of skylight reflections and residual sunglint are the subject of continuing study.

4. Computer Simulations

A. Simulation Reflectance Model

As previously discussed in Section 2, the accuracy of the polarization technique depends on the linear relation between $R_d(\lambda)$ and $R_s(\lambda)$, or on the linear relation between polarization components of reflectance spectra $R_\parallel(\lambda)$ and $R_\perp(\lambda)$ if $R_d(\lambda)$ becomes too small. In our original simulations,[19] a Mie scattering model was used to analyze the regions of applicability for this condition. The analysis was limited to a single particle size distribution and one algae component. However, that model can at best be described as approximate. In this section, a full atmosphere–ocean coupled vector radiative transfer program[22,32] based on the adding–doubling method is used to determine the polarization state of the water-leaving radiance. To support coastal water simulations, the inherent scattering and absorption properties due to detritus particles, mineral particles, and CDOM were included in our numerical experiments.

The resulting computations provide the complete Stokes vector $\boldsymbol{I} = \{I, Q, U, V\}$ for the total upwelling radiance just above the ocean surface as well as for

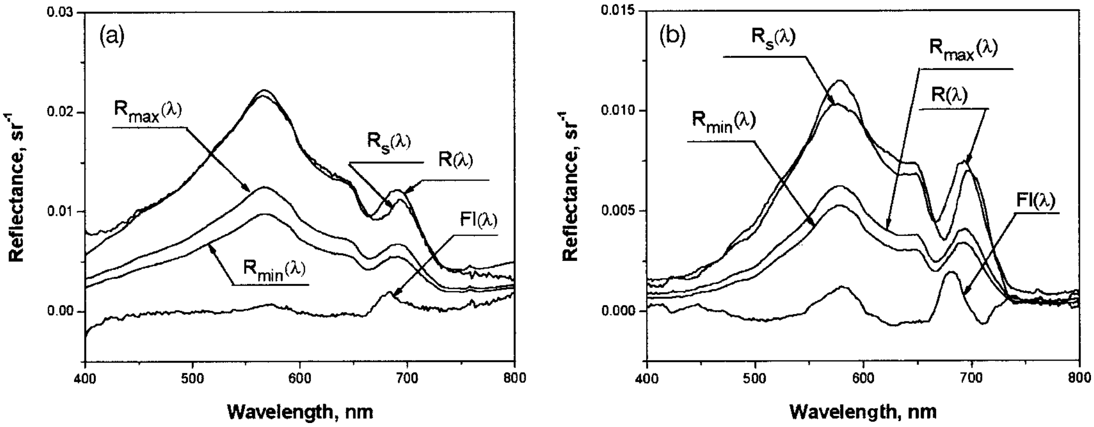

Fig. 10. Detected and processed spectra for the measurements in the field. (a) Shinnecock Bay, Long Island, Sun zenith angle of 61°, probe above water in vertical position, [Chl] = 8 mg/m^3; (b) Chesapeake Bay, Sun zenith angle of 20°, probe just below water at 45°, [Chl] = 41 mg/m^3.

the water leaving radiance contribution. A homogeneously mixed layer of molecules and aerosols with an aerosol optical thickness of 0.1 at $\lambda = 500$ nm was assumed for the atmosphere. The ocean layer contained three types of particle: phytoplankton, detritus, and minerals. A Junge distribution was assumed with the slope of -4 for all three types of particle over a size range from 0.1 to 50 μm and real refractive indices relative to water of 1.06, 1.04, and 1.18, respectively. The scattering matrices for these particles were derived from Mie computations, and appropriate fractions of each component were used to compile the effective scattering matrix of oceanic particulates. The underwater light absorption was modeled by the sum of absorption coefficients for pure water, phytoplankton, and detritus particles for open ocean waters. Absorption by CDOM and mineral particles was included for scattering of light in coastal waters. The ocean bottom reflection albedo, assumed Lambertian, varied from 0 to 0.5. The number of concentrations of the particulate matter used for open ocean waters are shown in Table 1. They were determined using the particle composition of Stramski *et al.*[33] with the modifications in the number concentrations in accordance with Morel.[34] To examine the influence of increased [Chl] on the polarization components, relationships typical for the open ocean were extended to the high [Chl] values (up to 80 mg/m^3). It should be pointed out that this partitioning leads to some overestimation of the mineral fraction in comparison to the regular values for open ocean waters. For coastal waters, fractions were varied according to the concentrations of phytoplankton and mineral particles, which are discussed in Subsection 4.C. The ocean optical thickness was fixed at 4.6 (optically deep, with less than 1% light reaching the bottom) except for the shallow-water cases in which the effect of the bottom was analyzed. The ocean surface roughness was modeled according to Cox and Munk[35] for wind speeds varying between 1.37 to 18.9 m/s. The analysis was limited to a solar zenith angle of 40° and in most cases to a nadir viewing position of the probe. This scattering geometry corresponds to an underwater light incident angle of $\theta_w \approx 30°$ for direct sunlight illumination and to a corresponding underwater light single scattering angle of $\Theta_w = 150°$. The collecting probe was taken to be just above the ocean surface.

B. Modeling of Fluorescence Spectra and its Retrieval From Reflectance Spectra Through Polarization

Estimation of the fluorescence spectra emitted from the water for given fluorescence efficiency requires analysis of absorption of light by algae and the total absorption between $\lambda = 400$ and 675 nm, the range of which defines the transformation of photosynthetically available radiation (PAR) into photosynthetically usable radiation (PUR) and reabsorption of fluorescence in the water.[1,11] The fluorescence energy is proportional to [Chl] and is represented as

Table 1. Number of Phytoplankton, Detritus, and Mineral Particles/m^3 Used in RT Simulations for Different [Chl] Concentrations

[Chl] mg/m^3	Phytoplankton	Detritus	Minerals	Total
0.01	1.30×10^{11}	1.29×10^{13}	5.24×10^{12}	1.82×10^{13}
0.2	2.60×10^{12}	8.25×10^{13}	3.36×10^{13}	1.19×10^{14}
5	6.50×10^{13}	2.92×10^{14}	1.19×10^{14}	4.76×10^{14}
20	2.60×10^{14}	3.71×10^{14}	1.51×10^{14}	7.83×10^{14}
40	5.20×10^{14}	3.25×10^{14}	1.32×10^{14}	9.77×10^{14}
80	1.04×10^{16}	1.22×10^{14}	4.95×10^{13}	1.06×10^{16}

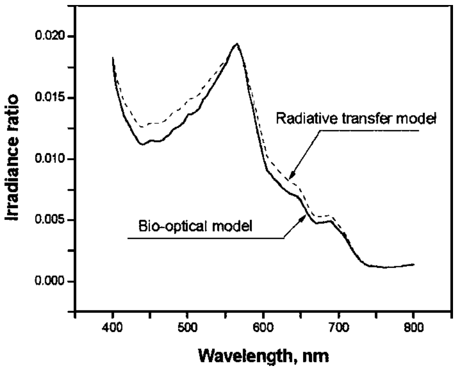

Fig. 11. Irradiance ratio spectra calculated by bio-optical model and the vector radiative transfer code for waters with [Chl] = 20 mg/m^3.

$$E_{\mathrm{Fl}} = \eta[\mathrm{Chl}]\int_{400}^{675} [E_d(\lambda)a_{\mathrm{ph}}'(\lambda)/a(\lambda)]\mathrm{d}\lambda, \qquad (10)$$

where η is the fluorescence efficiency, $E_d(\lambda)$ is the downwelling irradiance, and $a_{\mathrm{ph}}'(\lambda)$ is the [Chl]-specific (i.e., per unit [Chl]) absorption. After taking into account fluorescence reabsorption,[1] considering only emission into the upper hemisphere, and assuming $\eta = 0.03$, we modeled the fluorescence spectrum $\mathrm{Fl}(\lambda)$ as a Gaussian shape centered at 685 nm with a FWHM of 25 nm. The area under this shape was equal to the emitted fluorescence energy, and we normalized the $\mathrm{Fl}(\lambda)$ spectrum by the downwelling irradiance $E_d(\lambda)$.

It must be emphasized that fluorescence was not included in the radiative transfer model. To simulate the retrieval of the fluorescence, the fluorescence spectrum $\mathrm{Fl}(\lambda)$ as described above was split equally and superimposed on the orthogonal components $R_\perp(\lambda)$ and $R_\parallel(\lambda)$ derived from the radiative transfer computations of Stokes parameters I and Q for observations in the scattering plane. The reflectance components $R_{\max}(\lambda)$ and $R_{\min}(\lambda)$ were subsequently calculated according to Eqs. (1) and (2), and inverted back into the $\mathrm{Fl}(\lambda)$ spectra using Eq. (9). The regression was performed in the chlorophyll fluorescence free spectral bands of $\lambda = 400$ to 450 nm, 600 to 650 nm, and 750 to 800 nm. Note that these bands are also minimally affected by CDOM fluorescence.[6,36] The input fluorescence spectrum $\mathrm{Fl}(\lambda)$ was varied in these retrievals according to changes in [Chl] between 5 and 80 mg/m^3.

C. Results of Simulations

To test the radiative transfer model, its numerical results were compared for the irradiance ratio A just below the surface with those obtained from a general bio-optical model for open ocean waters. The bio-optical model values were derived from Morel and Prieur,[37]

$$A(\lambda) = 0.33b_b/a, \qquad (11)$$

where

$$b_b(\lambda) = 0.5b_w(\lambda) + \{0.002 + 0.02(0.5 - 0.25^* \ln[\mathrm{Chl}]) \times (550/\lambda)\}\{0.30[\mathrm{Chl}]^{0.62} - b_w(550)\} \qquad (12)$$

is the total backscattering coefficient,[26,34] b_w is the seawater scattering coefficient, and a is the total absorption coefficient that for a CDOM-free ocean is given by Morel,[38]

$$a(\lambda) = a_w(\lambda) + 0.06a_c^*(\lambda)[\mathrm{Chl}]^{0.65}. \qquad (13)$$

In Eq. (13), a_w is the absorption coefficient of pure water and a_c^* is the statistically derived [Chl]-specific absorption coefficient normalized to the chlorophyll absorption at 440 nm. The results in Fig. 11 show good agreement between the shapes of the irradiance ratio spectra predicted by the bio-optical model where the use of Eqs. (11)–(13) was extended to the higher [Chl] values and those provided by the RT computations.

It is important to realize that the degree of underwater light linear polarization P_w reaches its maximum at a single-scattering angle Θ_w of about 90° for an average in open ocean waters. In our case, $\Theta_w \approx 150°$, which leads to $P_w \approx 10\%$.[24,39] Since the fluorescence retrieval technique essentially uses P_w

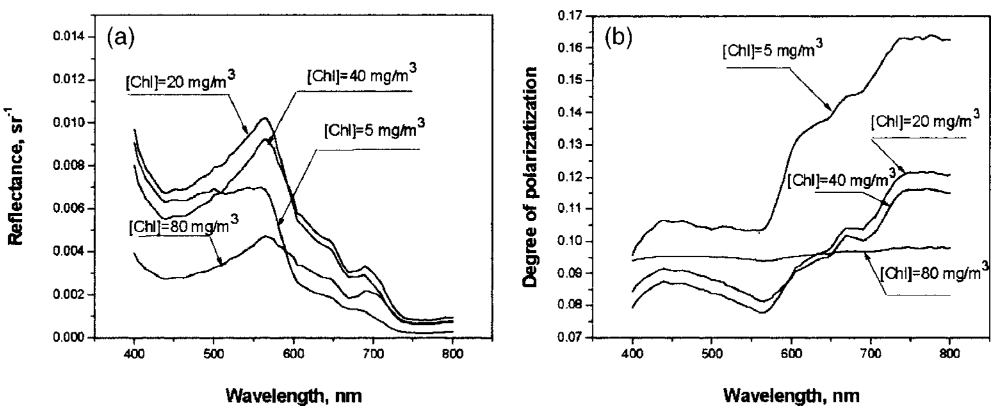

Fig. 12. (a) Spectra of reflectance, (b) degree of polarization for [Chl] = 5, 20, 40, and 80 mg/m^3.

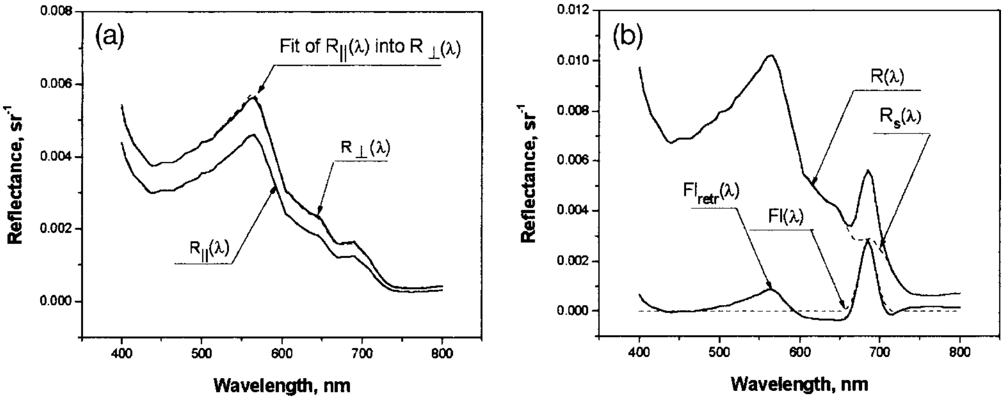

Fig. 13. (a) Spectra of $R_{\perp}(\lambda)$, of $R_{\|}(\lambda)$, and of the fit of $R_{\|}(\lambda)$ onto $R_{\perp}(\lambda)$. (b) Results of fluorescence retrieval for [Chl] = 20 mg/m^3.

to identify contributions from elastic scattering, changes in the magnitude of P_w will significantly affect the accuracy of this retrieval. We first examined variations of this accuracy for light emerging from waters dominated by algae. Although such conditions are typical for open ocean waters, [Chl] of 5 mg/m^3 and higher are more likely to appear in coastal zones. Figure 12 shows the water-leaving reflectance without superimposed fluorescence and its degree of linear polarization for waters with [Chl] = 5, 20, 40, and 80 mg/m^3. It is observed that this degree varies between 8% and 16%, which is sufficiently large for the separation and retrieval of fluorescence.

Results for the retrieval of $R_{\perp}(\lambda)$ and $R_{\|}(\lambda)$, as well as for the retrieval of fluorescence, are presented in Fig. 13 for [Chl] = 20 mg/m^3. Figure 13(a) shows an accurate fit of elastic component $R_{\|}(\lambda)$ into $R_{\perp}(\lambda)$. Figure 13(b) shows that chlorophyll fluorescence can be extracted with high accuracy for $\lambda > 650$ nm. There are, on the other hand, large errors in the retrieved fluorescence spectrum for the green part of the spectrum. These errors are caused by small deviations in linear relation between $R_{\perp}(\lambda)$ and $R_{\perp}(\lambda)$ that are subsequently amplified by the small denominator in Eq. (9).

To see how accurate the polarization-based retrieval of fluorescence can be, the fluorescence height $\mathrm{Fl}_{\mathrm{retr}}$ [defined as Fl(685)–Fl(650)] was derived from this retrieval and compared with the theoretical input and with the baseline-method derived fluorescence $\mathrm{Fl}_{\mathrm{baseline}}(685)$. The results of this comparison are shown in Fig. 14. It is seen that while polarization discrimination and baseline methods provide fluorescence line heights that correlate well with the theoretical (input) values, the baseline approach systematically overestimates the fluorescence height by at least 5%−10%. While this leads to a slight underestimation of the elastic backscatter spectrum, and hence of the [Chl] value from NIR spectra, it can be relatively easily corrected. It should be pointed out that while extracting the fluorescence line height is important, the fluorescence height itself is not a complete indicator of [Chl] because of the dependence of fluorescence efficiency on illumination and environmental factors that can vary considerably.

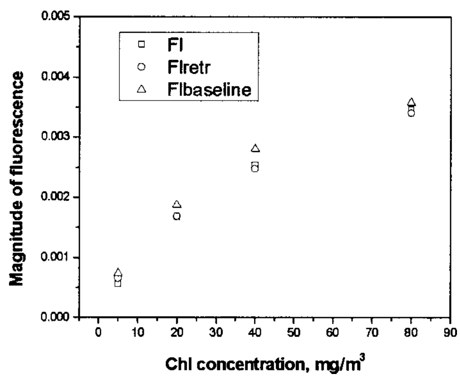

Fig. 14. Comparison between the input fluorescence value and the corresponding polarization-retrieved and baseline-retrieved values.

We now consider the effect of ocean surface roughness on the polarization-based retrieval of fluorescence. Figure 15 shows that while the total reflectance spectra increases as the surface wind speed increases from 1.4 to 18.9 m/s, the corresponding degrees of polarization decrease (but stay within the same range 8%−16%) in the NIR. We note, however, that these results pertain to average ocean surface wave slopes. To get similar results in field measurements, one should average measurements of the reflectance spectra taken over a time period of several seconds to minimize noise and fluctuations as were done in both laboratory and field tests.

Finally, we examined the effect of ocean bottom albedo on the polarization-based retrieval of fluorescence. We assumed this bottom to be unpolarizing and modeled it as a Lambertian reflector. Here we found the potential for significant influence on the accuracy of the polarization-derived fluorescence spectrum. In particular, when the ocean is not optically deep, a significant portion of the downwelling underwater light field reaches the bottom. If, in addition, the albedo of this bottom is larger than 0.1, the light reflected by this bottom can contribute significantly to the water-leaving radiances. The latter contribution causes the degree of linear polarization of these radiances to decrease markedly. We found this to occur for depths ranging from 1 to 20 m and for

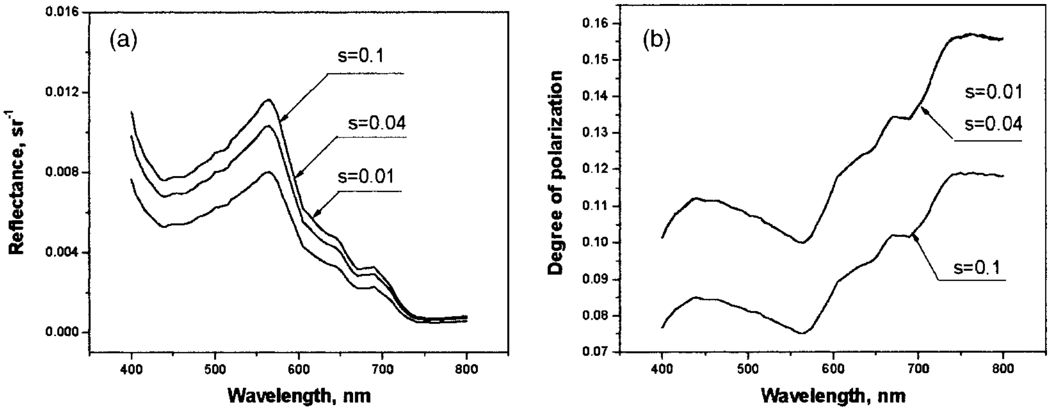

Fig. 15. (a) Polarized total reflectance spectra and (b) degree of polarization for [Chl] = 20 mg/m^3, and ocean surface wind speeds ranging from 1.37 to 18.9 m/s (surface roughness parameter S = 0.01–0.1; S = 2s^2, where s is the surface slope variance for a Gaussian surface slope distribution).

[Chl] = 20 mg/m^3. Figure 16 shows the accompanying large increase in total reflectance.

While it is clear that the bottom reflection of underwater light degrades the degree of linear polarization of water-leaving radiances, one should remember that we conducted our sensitivity study for a fairly difficult scattering geometry, i.e., for a small Sun angle and nadir viewing that leads to an underwater light single-scattering angle of 150°. The polarization of underwater light scattered at such angles is already quite small and hence easily masked by the unpolarized nature of light reflected by the bottom. More favorable scattering geometries can be obtained by viewing the scattering plane off the nadir direction. Such geometries lead to larger polarization degrees of water-leaving radiances (provided that the polarization caused by ocean surface transmission remains small), and hence to more accurate retrieval of fluorescence spectra with polarization-based retrieval methods.

D. Modification of the Simulation Model for Coastal Waters and Simulation Results

In coastal waters, concentrations of mineral particles can dominate the scattering process and CDOM concentrations can increase the total absorption coefficient significantly. Note that these concentrations often do not covary with [Chl]. The total absorption coefficient for such waters can be modeled by[33,38]

$$a(\lambda) = a_w(\lambda) + a_{\mathrm{ph}}(\lambda) + N_{\min}\sigma_{a,\min}(\lambda) + a_y(\lambda), \quad (14)$$

where $a_{\mathrm{ph}}(\lambda)$ is the absorption of algae, $N_{\min}$ is the particle concentrations, $\sigma_{a,\min}(\lambda)$ is the absorption cross section of mineral particles, $a_w(\lambda)$ is the absorption of pure water, and $a_y(\lambda)$ is the absorption of yellow matter (CDOM). Algae absorption can be calculated according to Eq. (13). Absorption of yellow matter can be obtained[26] from $a_y(\lambda) = a_y(\lambda_0) \exp[-0.014(\lambda - \lambda_0)]$ where $a_y(\lambda_0)$ is the absorption of the yellow matter at a reference wavelength λ_0. In our calculations, we choose $a_y(\lambda_0) = 0.5$ for $\lambda_0 = 440$ nm.

We considered the same set of particles as in previous simulations but varied the particulate fractions with [Chl] = 20 mg/m^3 and concentrations of mineral particles $[C_s]$ = 10, 40, and 100 mg/l, which correspond to the number of mineral particles/m^3 3.36×10^{15}, 1.3×10^{16}, 3.36×10^{16}, respectively. We used, for the latter particles, a real part of the refractive index of 1.18 and a density of 2600 kg/m^3. The absorption coefficient of mineral particles was calculated as $a_s(\lambda) = a_s(\lambda_0)\exp[-0.009(\lambda - \lambda_0)]$, where $a_s(\lambda_0) = 0.01263[C_s]$ for $\lambda_0 = 440$ nm.[8]

Simulations for the conditions described above with a vertically positioned probe show that as a result of scattering by the mineral particles, the degree of linear polarization for water-leaving radiances can become small, will result in the increase of noise, and make the fluorescence retrieval more difficult or unreliable. To increase this degree, we reduced the underwater light single-scattering angle from 150° to 128° by changing the viewing angle above the water from 0° to 30°. Results for the simulated reflectance with and without superimposed fluorescence as well as for degree of polarization are shown in Fig. 17. Note that the degree of polarization is now of the order of 10% even for the high concen-

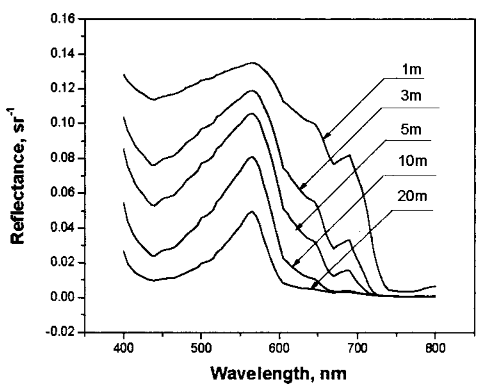

Fig. 16. Reflectance for an ocean layer with [Chl] = 20 mg/m^{3}as a function of depths. The ocean bottom albedo and surface wind speed for these cases are 0.5 and 7.2 m/s, respectively. Fluorescence component is not included.

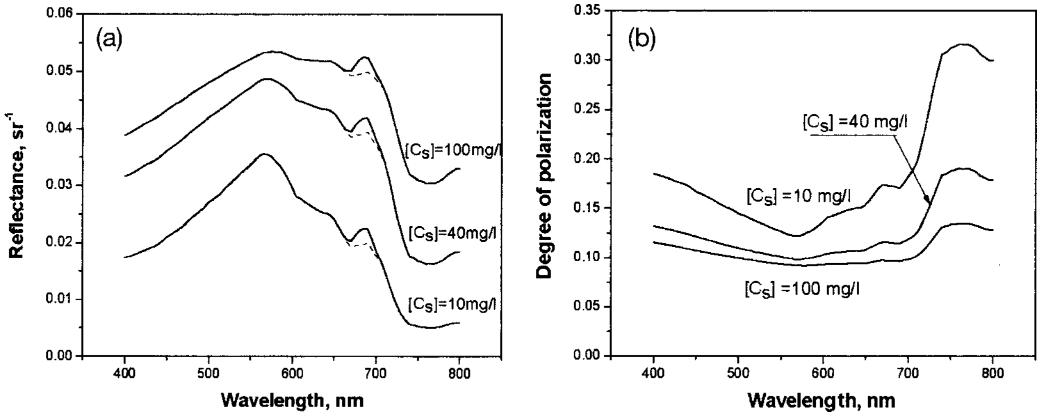

Fig. 17. (a) Reflectance with (solid curves) and without (dotted curves) superimposed fluorescence. (b) The corresponding degree of polarization for [Chl] = 20 mg/m^3 and concentration of minerals $[C_s] = 10, 40,$ and 100 mg/l.

trations of minerals, which allows fluorescence to be retrieved successfully. This shows that attention should be paid to the probe orientation when extracting polarized signals in coastal waters. However, in simulations for concentrations of mineral particles $[C_s] = 10$ mg/l and viewing angles in the range $0°-40°$ fluorescence was successfully retrieved, which supports the experimental results in Subsection 3.C. It should be pointed out that to properly scale fluorescence retrievals obtained at different viewing geometries, appropriate geometric corrections need to be applied. Figure 17 also shows that the degree of polarization exhibited a strong dependence on mineral particle concentration and is a useful property to consider in future retrievals using sensors with polarization analyzing capabilities.

Finally, we note that while the superimposed fluorescence was kept the same for all three concentrations of minerals, it can actually decrease for high mineral concentrations because of an increase in absorption.[20] Our simulations show further that the fluorescence height over baseline method leads to a strong overestimation of fluorescence for such concentrations (Fig. 18).

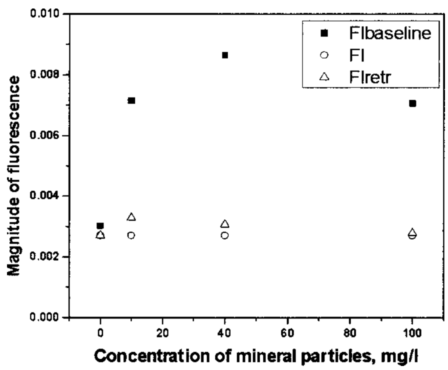

Fig. 18. Comparison between the input fluorescence value and the corresponding polarization-retrieved and baseline-retrieved values for coastal waters.

5. Conclusions

The laboratory results presented here demonstrate the essential elements of the polarization discrimination technique and its applicability to different types of algae, for a wide variety of illumination and water conditions, including high mineral particle concentrations (TSS), rough surface water conditions, and natural sunlight. The experimental work was extended to field measurements in eastern Long Island waters and in the Chesapeake Bay, where fluorescence extraction by polarization discrimination is demonstrated for coastal waters. An analysis was then carried out to examine if these results could be simulated theoretically, and to define the scope and limitations of the technique. For this analysis, we assessed the efficacy of the fluorescence retrieval by simulating the total and polarized components of water-leaving radiances originating from elastic scattering and fluorescence in open ocean and coastal waters using a vector radiative transfer code, and superimposing the contribution of known fluorescence spectra onto calculated elastic reflectance for open ocean and coastal waters. The RT code was tested against conventional bio-optical models and shown to be spectrally in good agreement. The total resulting spectral data were then processed by the polarization discrimination procedure to retrieve the apparent fluorescence spectra. It was found that the retrieval algorithm gives good results for both open ocean and coastal waters, permitting accurate extraction of fluorescence with less than 10% error depending on the chlorophyll concentration and the water composition. Limitations of the method are encountered when bottom reflectance and high concentration mineral multiple scattering are major contributors. To improve retrieval accuracy under such circumstances requires a change in viewing angle such that the underwater light single-scattering angles becomes closer to 90° where polarization of scattered light is largest.

The fluorescence heights obtained by the polarization-based retrieval method were also compared with those obtained by the traditional baseline subtraction methods and found to be more accurate. The radiative transfer analyses discussed showed that the traditional height over baseline fluorescence extraction method strongly overestimates the fluorescence values, particularly for coastal waters, where the baseline retrieved fluorescence height erroneously increases with concentration of mineral particles due to scattering or absorption changes that bias the baseline. This effect is more significant for lower fluorescence efficiencies and needs to be taken into account in algorithms utilizing fluorescence height.

This research has been supported by grants from NASA and NOAA. We thank E. Boss and an anonymous reviewer for their valuable comments and suggestions, which led to significant improvements in this paper.

References

1. J. F. R. Gower, R. Doerffer, and G. A. Borstad, "Interpretation of the 685 nm peak in water-leaving radiance spectra in terms of fluorescence, absorption and scattering, and its observation by MERIS," Int. J. Remote Sens. **20,** 1771–1786 (1999).
2. A. A. Gitelson, Y. Z. Yacobi, D. C. Rundquist, R. Stark, L. Han, and D. Etzion, "Remote estimation of chlorophyll concentration in productive waters: principals, algorithm development, and validation," in *Proceedings of NWQMC, National Monitoring Conference* (Austin, Texas, 2000), pp. 149–160.
3. G. Dall'Olmo and A. A. Gitelson, "Effect of bio-optical parameter variability on the remote estimation of chlorophyll-a concentration in turbid productive waters: experimental results," Appl. Opt. **44,** 412–422 (2005).
4. J. F. Schalles and C. M. Hladik, "Remote chlorophyll estimation in coastal waters with tripton and CDOM interferences," in *Proceedings of the Ocean Optics XVII Conference* (Fremantle, Australia, 2004).
5. K. H. Szekielda, C. Gobler, B. Gross, F. Moshary, and S. Ahmed, "Spectral reflectance measurements of estuarine waters," Ocean Dyn. **53,** 98–102 (2003).
6. D. Pozdnyakov, A. Lyaskovsky, H. Grassl, and L. Petterson, "Numerical modeling of transspectral processes in natural waters: implications for remote sensing," Int. J. Remote Sens. **23,** 1581–1607 (2002).
7. S. B. Wozniak and D. Stramski, "Modeling of the optical properties of mineral particles suspended in seawater and their influence on ocean reflectance and chlorophyll estimation from remote sensing algorithms," Appl. Opt. **43,** 3489–3503 (2004).
8. D. Doxaran, J. M. Froidefond, S. Lavender, and P. Castaing, "Spectral signature of highly turbid waters. Application with SPOT data to quantify suspended particulate matter concentrations," Remote Sens. Environ. **81,** 149–161 (2002).
9. M. Sydor and R. Amone, "Effect of suspended particulate and dissolved organic matter on remote sensing of coastal and riverine waters," Appl. Opt. **36,** 6905–6912 (1997).
10. L. Han, D. C. Rundquist, L. L. Liu, R. N. Fraser, and J. F. Schalles, "The spectral responses of algal chlorophyll in water with varying levels of suspended sediment," Int. J. Remote Sens. **15,** 3707–3718 (1994).
11. M. Babin, A. Morel, and B. Gentili, "Remote sensing of sea surface Sun-induced chlorophyll fluorescence: consequences of natural variations in the optical characteristics of phytoplankton and the quantum yield of chlorophyll a fluorescence," Int. J. Remote Sens. **17,** 2417–2448 (1996).
12. C. Hu, F. E. Muller-Karger, C. J. Taylor, K. L. Carder, C. Kelble, E. Johns, and C. A. Heil, "Red tide detection and tracing using MODIS fluorescence data: a regional example in SW Florida coastal waters," Remote Sens. Environ. **97,** 311–321 (2005).
13. C. Hu and K. J. Voss, "Measurements of solar-stimulated fluorescence in natural waters," Limnol. Oceanogr. **43,** 1198–1206 (1998).
14. E. Fuchs, "Separating the fluorescence and reflectance components of coral spectra," Appl. Opt. **40,** 3614–3621 (2001).
15. F. Grum, "Colorimetry of fluorescent materials," in *Optical Radiation Measurements* (Academic, 1980), Vol. 2, Chap. 6.
16. C. S. Roesler and M. J. Perry, "*In situ* phytoplankton absorption, fluorescence emission, and particulate backscattering spectra determined from reflectance," J. Geophys. Res. **100,** 13279–13294 (1995).
17. J. Fischer and U. Kronfeld, "Sun-stimulated chlorophyll fluorescence. 1. Influence of oceanic properties," Int. J. Remote Sens. **11,** 2125–2147 (1990).
18. S. R. Laney, R. M. Letelier, and M. R. Abbott, "Parameterizing the natural fluorescence kinetics of *Thalassiosira weissflogii,*" Limnol. Oceanogr. **50,** 1499–1510 (2005).
19. S. Ahmed, A. Gilerson, A. Gill, B. M. Gross, F. Moshary, and J. Zhou, "Separation of fluorescence and elastic scattering from algae in seawater using polarization discrimination," Opt. Commun. **235,** 23–30 (2004).
20. A. Gilerson, J. Zhou, B. Elmaanaoui, B. Gross, F. Moshary, and S. Ahmed, "Separation of fluorescence and scattering from algae and suspended solids in seawater through polarization: modeling and experiments," in *Proceedings of the Eighth International Conference on Remote Sensing for Marine and Coastal Environments* (Halifax, Nova Scotia, Canada, 2005).
21. A. Gilerson, M. Oo, J. Chowdhary, B. M. Gross, F. Moshary, and S. A. Ahmed, "Polarization characteristics of water-leaving radiance: application to separation of fluorescence and scattering components in coastal waters," in *Remote Sensing of the Coastal Oceanic Environment,* R. J. Frouin, M. Babin, and S. Sathyendranath, eds., Proc. SPIE **5885,** 95–105 (2005).
22. J. Chowdhary, B. Cairns, and L. D. Travis, "The contribution of the water-leaving radiances to multiangle, multispectral polarimetric observations over the open ocean: bio-optical model results for case I waters," Appl. Opt. **45,** 5542–5567 (2006).
23. J. Chowdhary, B. Cairns, M. I. Mishchenko, P. V. Hobbs, G. F. Cota, J. Redemann, K. Rutledge, B. N. Holben, and E. Russell, "Retrieval of aerosol scattering and absorption properties from photopolarimetric observations over the ocean during the CLAMS experiment," J. Atmos. Sci. **62,** 1093–1117 (2005).
24. M. Chami, R. Santer, and E. Dilligeard, "Radiative transfer model for the computation of radiance and polarization in an ocean–atmosphere system: polarization properties of suspended matter for remote sensing," Appl. Opt. **40,** 2938–2416 (2001).
25. C. F. Bohren and D. R. Huffman, *Absorption and Scattering of Light by Small Particles* (Wiley, 1983).
26. C. D. Mobley, *Light and Water: Radiative Transfer in Natural Waters* (Academic, 1994).
27. S. Ahmed, A. Gilerson, A. Gill, B. M. Gross, F. Moshary, and J. Zhou, "Polarization technique for separating overlapping fluorescence and reflectance spectra applied to algae in seawater in the presence of suspended matter," in *Proceedings of the Ocean Optics XVII Conference* (Fremantle, Australia, October 25–29, 2004).
28. R. M. Letelier and M. R. Abbott, "An analysis of chlorophyll fluorescence algorithms for the moderate resolution imaging spectrometer (MODIS)," Remote Sens. Environ. **58,** 215–223 (1996).
29. J. R. V. Zaneveld, E. Boss, and P. A. Hwang, "The influence of coherent waves on the remotely sensed reflectance," Opt. Express **9,** 260–266 (2001).

30. H. R. Gordon, "Normalized water-leaving radiance revisiting the influence of surface roughness," Appl. Opt. **44,** 241–248 (2005).
31. B. Fougnie, R. Frouin, P. Lecomte, and P. Y. Deschamps, "Reduction of skylight reflection effects in the above-water measurement of diffuse marine reflectance," Appl. Opt. **38,** 3844–3856 (1999).
32. J. F. De Haan, P. B. Bosma, and J. W. Hovenier, "The adding method for multiple scattering calculations of polarized light," Astron. Astrophys. **183,** 371–397 (1987).
33. D. Stramski, A. Bricaud, and A. Morel, "Modeling the inherent optical properties of the ocean based on the detailed composition of the planctonic community," Appl. Opt. **40,** 2929–2945 (2001).
34. A. Morel, "Optical modeling of the upper ocean in relation to its biogenuous matter content (Case 1 waters)," J. Geophys. Res. **93,** 10749–10768 (1988).
35. C. Cox and W. Munk, "Statistics of the sea-surface derived from sun-glitter," J. Mar. Res. **13,** 198–227 (1954).
36. S. A. Green and N. V. Blough, "Optical absorption and fluorescence properties of chromophoric dissolved organic matter in natural waters," Limnol. Oceanogr. **39,** 1903–1916 (1994).
37. A. Morel and L. Prieur, "Analysis of variations in ocean color," Limnol. Oceanogr. **22,** 709–722 (1977).
38. A. Morel, "Light and marine photosynthesis: a spectral model with geochemical and climatological implications," Prog. Oceanogr. **26,** 263–306 (1991).
39. K. J. Voss and E. S. Fry, "Measurement of the Mueller matrix for ocean water," Appl. Opt. **23,** 4427–4439 (1984).